37th Executive Secretariat
Via G. Agusta 520
21017 Cascina Costa di Samarate (VA) Italy
Phone: +39 0331 0331 229719
Fax: +39 0331 229508
E-mail: erf2011@agustawestland.com

Paper Number: 137

ELECTROMAGNET DRIVING FORCE FOR ACTIVE GURNEY FLAP: FINITE ELEMENT MODELING AND PRELIMINARY EXPERIMENTAL VALIDATION

G. Diodati, M. Ciminello, A. Concilio
CIRA, Via Maiorisi, 81043 Capua (CE), Italy

Active Rotor Technologies would enable a helicopter to operate for instance with a reduced tip speed of its main rotor whilst preserving current flight performance capabilities. A range of potential technologies could be incorporated within segments of a helicopter main rotor blade to meet those requirements. According to authors' opinion, an 'Active' Gurney Flap (AGF) offer significant potential through the possibility of 'conditioning' the performance of rotor blades by allowing the implementation of different geometries (extended / retracted) as the blade rotates around the helicopter.
An innovative way to realize an AGF, based on an electro-magneto-mechanical system made of a flapped beam and electromagnet actuators is presented. This idea could be implemented in a typical space available on standard blade profiles (like NACA23012) and allow a perpendicular protrusion of the device.
Preliminary numerical and experimental results were obtained in the Smart Structures Lab of the Italian Aerospace Research Centre (CIRA) which proposed and is currently developing the concept. Experimental and numerical deployment time were reported and a continuous two-hour test was performed to highlight the capability of the device to work cyclically.

INTRODUCTION

Conventionally, a Gurney Flap is a small "tooth", perpendicular to the lower surface of the aerofoil and located at its trailing edge area. An Active GF is essentially a Gurney Flap with the ability to alter its height from zero (fully retracted) to a maximum (fully extended). Its impact upon the performance can be varied and controlled as the rotor blade rotates. Actuating such devices during rotor blade rotation allows improving flow features on the retreating side while does not affect the blade performance on the advancing side. Enhancement of lift and general features of the rotor blade are given by the generation of two contra-rotating vortices behind the flap, which alter Kutta condition and circulation in the region, (ref. [1]). The new circulation arrangement keeps the flow attached to the profile, and thus permits achieving higher angles of attack, without creating a gap in the flow and then stall (ref. [2] – ref. [7]).
Recently, several suitable actuator solutions were presented taking into account requirements such as bandwidth and weight. In ref. [8], piezoelectric devices ranging from stacks and patches to linear ultrasonic actuators, all commercially available, were compared at level of their respective performance. Linear actuator was found to be much lighter than stack actuator solutions. The latter devices however were shown to have a better bandwidth, allowing both a full Gurney flaps deployment along the blade rotation, and the implementation of active vibration reduction systems in a range up to 4×rev (ref. [8]).
The authors, ref. [9], evaluated the performance of three different AGF mechanisms, referring to a basic architecture using a simple cantilever beam. Piezo patch actuators resulted inadequate to produce required displacement. Stack actuators were proved to achieve the desired behaviour, but power consumption and added weight penalties seemed excessive for actual rotorcraft applications. The one based on electromagnet actuators seemed the most promising actuation system. At the first early stage of the study, tests showed the desired structural dynamic response was attained, with a limited electrical power consumption (less than 5W) and a low weight penalty (about 50 gr). The originality and advantage of this concept led the authors to set-up a preliminary prototype beam flap and the relative FE model. Experimental activities were aimed at validating finite element numerical predictions (the effect of centrifugal forces were not considered at this stage).

AGF PRELIMINARY REQUIREMENTS

Main rotor major characteristics, considered in the herein reported investigation, are following summarized:

- Number of blades: 4

- Radius: about 8 m
- Tip speed: about 200.0 m/s

A centrifugal force of about 70g per blade span meter then resulted, giving rise to an acceleration of about 560g at the blade tip. In a rotor blade, thicker profiles are generally used at the root and thinner at the tip. Because stall control phenomena arises in the root region, only root profiles are referred to. In the current application, NACA23012 was selected, Figure 1.

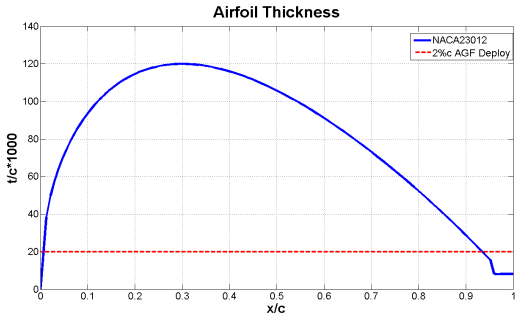

Figure 1: Profile thickness

As reported in [10], the best AGF position is at the trailing edge; performance deteriorates as it is moved upstream. Good results can be however achieved up to 90% c, while no significant performance loss is shown up to 95% c. References [11] to [13] demonstrated that among a range between 1 and 2.5% c height devices, the shorter is the one showing the best performance. In this work, some preliminary aerodynamic investigations address the study towards a 2% c height AGF.

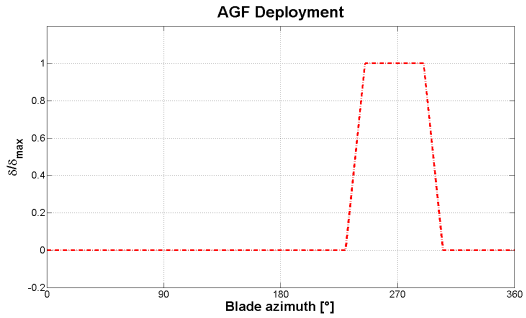

Figure 2: Tip deployment law

The law regulating the height of the actuator is fundamental in order to identify the dynamic characteristics of the actuation system. Such a deployment law can have a shape as the one reported in Figure 2. According to that, the AGF shall pass from a fully retracted to a fully extended state position in about 10° to 15° azimuth angle, corresponding to a period of about 10 ms to the referred angular speed. The actuation frequency may be instead fixed at about 4 Hz.

AGF STRUCTURAL SYSTEM MODELING

The basic structure adopted for the implementation of the following technological solution is a cantilever beam with a flap at the tip. This choice relies in the possibility of attaining the required performance in terms of flap deployment with a very simple structure. Thanks to the elasticity of the beam, in fact, such a dynamic response can be obtained without any kind of amplification system and avoiding hinges and sliding mechanisms, that in perspective could give problems in the centrifugal field, characteristic of typical helicopter rotor blades. The beam is hence driven by an electromagnetic force, opportunely placed and optimally dimensioned. The structural part of the AGF device is made of a second order system, excited by a concentrated magnetic force. According to the theory, the beam equation is:

$$EI\frac{\partial^4 Y(x,t)}{\partial x^4}+m\frac{\partial^2 Y(x,t)}{\partial t^2}=F(x,t) \qquad (1)$$

where E is the Young modulus, I the moment of inertia, m the mass per unit length, F the external force, Y the transversal displacement of the beam. If the first mode of the cantilever beam with an end mass is considered, the solution can be written as follows:

$$Y(x,t)=q(t)y(x) \qquad (2)$$

Where q and y are respectively the temporal law and the deformed shape of the first mode. If L_b is the length of the beam, it follows:

$$y(x)=(1-\frac{x}{L_b})^3-3(1-\frac{x}{L_b})+2 \qquad (3)$$

Substituting equations (2) and (3) into (1):

$$EI\frac{\partial^4 y(x)}{\partial x^4}q(t)+my(x)\frac{\partial^2 q(t)}{\partial t^2}=F(Y(x,t)) \qquad (4)$$

By means of spatial integration, equation Eq.(4) becomes:

$$\frac{\partial^2 q(t)}{\partial t^2}+\frac{\int_0^{L_b} EIy(x)\frac{\partial^4 y(x)}{\partial x^4}dx}{m\int_0^{L_b} y^2(x)dx}q(t)=\frac{\int_0^{L_b} y(x)F(Y(x,t))dx}{m\int_0^{L_b} y^2(x)dx} \qquad (5)$$

that is:

$$\frac{\partial^2 q(t)}{\partial t^2}+\omega_1^2 q(t)=\frac{y(x_F)F(Y(x_F,t))}{m\int_0^{L_b} y^2(x)dx} \qquad (6)$$

in fact:

$$\int y(x)F(q(t)y(x))\cdot\delta(x-x_F)dx=y(x_F)F(q(t)y(x_F)) \qquad (7)$$

therefore we obtain:

$$\ddot{q}(t) + \omega_1^2 q(t) = K \cdot F(q(t)) \tag{8}$$

where:

$$\omega_1 = \sqrt{\frac{3EI}{L_b^3 M}} = \sqrt{\frac{3EI}{L_b^3 (M_F + 0.24 M_b)}} \tag{9}$$

and

$$K = \frac{y(x_F)}{M_F + 0.24 M_b} \tag{10}$$

A Matlab routine was implemented and used to evaluate the previous equation in time domain. The beam excitation force is modelled according to what reported in the following paragraph. Results were used for comparison with experimental test rig data.

AGF MAGNETIC FORCE MODELING

In order to understand the behaviour of the magneto-mechanical system, magnetic fields were modelled and the resulting attracting forces produced by the electromagnet devices were derived. FEMM 4.2, ref. [14], was used to perform the abovementioned simulations. It is an open source suite of programs for solving low frequency electromagnetic problems on 2-D planar and axial-symmetric domains. A CAD-like interface is included for modelling the addressed system geometry and physics. Solutions can be displayed in the form of contour and density plots.

An electromagnet main characteristic is the electromagnetic holding force F_h, necessary for detaching a chunk of iron in a direction perpendicular to its surface. Fort a cylindrical electromagnet, this force depends on the following factors:

- Magnetic gap between the electromagnet and a regular piece of iron: the magnetic holding force is maximum when the two surfaces are perfectly adherent and smooth (magnetic gap zero).
- Thickness of the iron piece to be attracted: the electromagnetic force is maximum when the thickness S is higher than the inner diameter of the electromagnet.
- Electrical supply.

The main input data for FEMM4.2 were taken from datasheets, reporting main geometrical and physical properties of the selected device, ref. [15]. From these data, the circuit reluctance R could be computed by the following formula:

$$R = \frac{N \cdot J}{\Phi} \tag{11}$$

where N and J are the number of turns and current respectively, while the magnet flux linkage ϕ was derived from FEMM4.2 (see, for instance, Figure 3).

The actual magneto-motive force, $\mathcal{T}$ was then calculated from the classical expression, function of the holding force.

$$\mathcal{T} = \sqrt{2\mu_0 F_h R^2 S} \tag{12}$$

where S is the contact surface and μ_0 the magnetic permittivity in the air.

Comparisons were performed between attained numerical and datasheet values of the attraction force, computed as the gap varies.

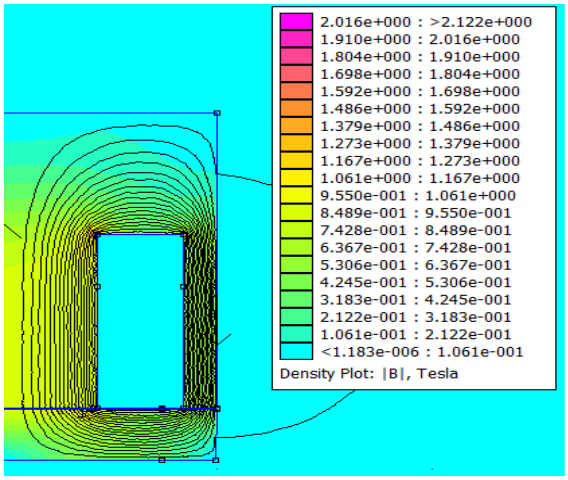

Figure 3: Simulation of the magnetic field lines and flux density

Results are reported in Figure 4, showing a good result agreement.

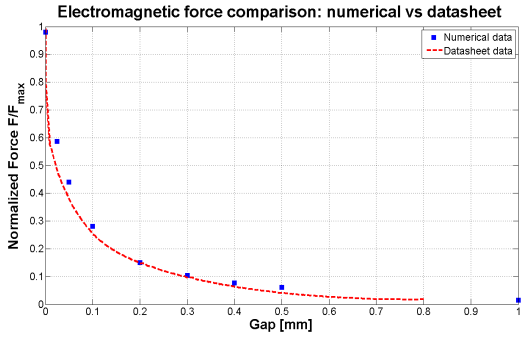

Figure 4: Numerical behaviour of the electromagnetic force Fh vs. air gap

FEMM4.2 computations, involving the full assembled system, supplied the excitation magnetic driving forces to be introduced in the Matlab dynamic model of the beam, implementing Eq. (8). Magnetic and elastic forces govern the dynamic response of the beam, then modulating the upper and lower level of protrusion.

Beam deployment δ/δ_{max}	Force (N)
0.001	2.06
0.036	1.48
0.073	1.19
0.136	0.88
0.227	0.61
0.318	0.44
0.409	0.35
0.500	0.29
0.591	0.25
0.682	0.23
0.773	0.20
0.864	0.18
0.982	0.09
1.000	0.03

Table 1: Finite element estimation of magnetic force vs. air gap

NUMERICAL AND EXPERIMENTAL TESTS

In order to compare numerical and experimental results, a simplified test rig, hosting a preliminary active beam prototype was realized.

A strain gauge sensor, bonded at the clamped edge of the beam, was used to retrieve the deployment time of the flap. At first, the test article did not include any damping treatment and the following time evolution is given in Figure 5.

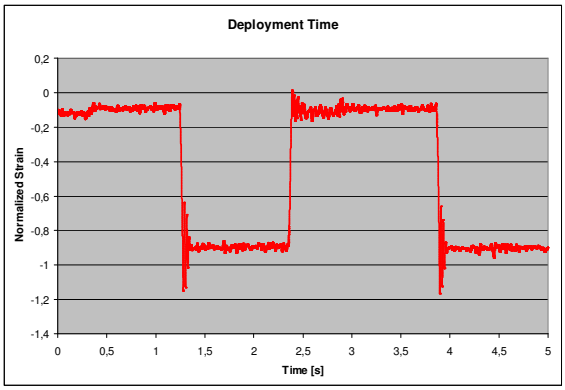

Figure 5: AGF deployment time without damp

The output signal was obtained through a non-automatic switch of the electromagnet. These measurements were aimed at evaluating the deployment and the retraction times of the flap.

In the next Figure 6 and Figure 7, localised zoom of Figure 5 are reported, emphasizing structural oscillations, following the beam blockage at the electromagnet positions.

In order to improve the quality of the dynamics a damping treatment was added to the system. To evaluate the beam equivalent viscous damping factor, ζ, the logarithmic decay technique was used.

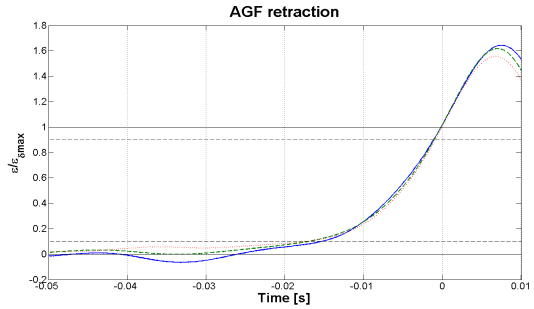

Figure 6: AGF without damping retraction

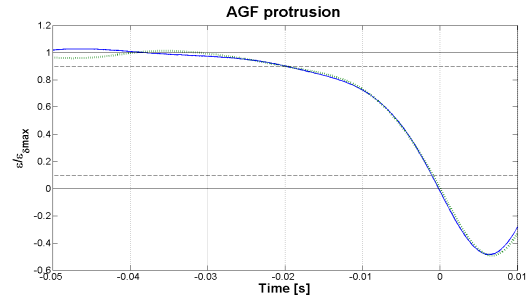

Figure 7: AGF without damping protrusion

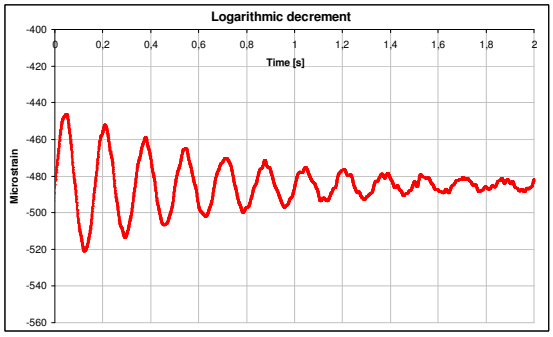

Figure 8: Beam free motion

The logarithm of the vibration amplitudes ratio at two successive maxima, Figure 8, is a measure of the viscous damping factor as follows:

$$\ln\left(\frac{x(t_1)}{x(t_2)}\right)=\frac{2\pi\xi}{\sqrt{1-\xi^2}} \qquad (13)$$

ξ	0.037
T (s)	0.166
f (Hz)	6.02

Table 2: Viscous damping coefficient and first resonance estimation

Measurements were then repeated. The new time history is reported in Figure 9. A smoothed dynamic response of the forced system arises. Some minor spikes, however, are still present. In order to evaluate AGF deployment time, computed

at protrusion and retraction, 10% and 90% nominal amplitude were used as threshold. Some results, referring to history reported in Figure 9, are summarised in Table 3.

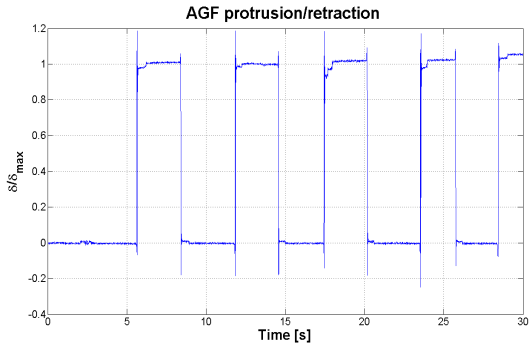

Figure 9: Damped AGF deployment tests

Retraction test	t_i (s)	t_f (s)	Δt (s)
1	5.617	5.629	0.012
2	11.820	11.830	0.010
3	17.430	17.440	0.010
4	25.750	25.760	0.010
Protrusion test	t_i (s)	t_f (s)	Δt (s)
1	8.405	8.412	0.007
2	14.570	14.580	0.010
3	20.170	20.180	0.010
4	28.450	28.460	0.010

Table 3: Damped AGF protrusion and retraction times

In what follows (Figures 10 and 11) a zoom of the previous Figure 9 are plotted. A better repeatability of the measures is evident together with a reduced overshoot. Numerical computation of the AGF deployment times was performed by using the electromagnetic force as calculated with FEMM 4.2 (Table 1). Eq. (8) was then solved by introducing the estimated structural damping, reported in Table 2. Matlab ODE45 routine was used to simulate the beam time response, implementing Runge–Kutta algorithm. Results are reported in Figure 12, showing 12 ms of retraction time.

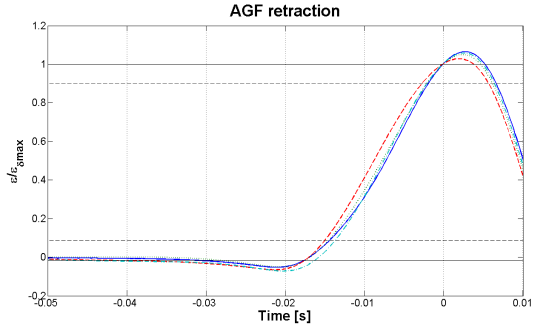

Figure 10: Damped AGF retraction

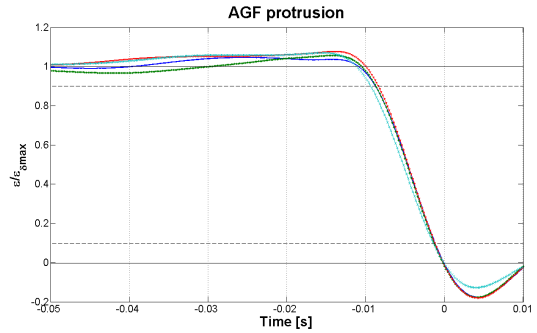

Figure 11: Damped AGF protrusion

Figure 12: Numerical estimation of AGF deployment time

Experimental and numerical results are collected in Table 4. Results show to be in a good agreement and repeatability.

Num. AGF retraction time	**12 ms**
Exp. AGF retraction time: test 1	**12 ms**
Exp. AGF retraction time: test 2	**10 ms**
Exp. AGF retraction time: test 3	**10 ms**
Exp. AGF retraction time: test 4	**10 ms**

Table 4: Numerical and experimental time comparison (10%-90% retraction)

ENDURANCE TESTS

In order to check the system behaviour preliminarily, under cycling load, an electronic board was manufactured to drive the electromagnet actuators at a desired frequency.

In the integrated circuit, a multi-vibrator device, the frequency and duty cycle can be controlled with two external resistors (R_A and R_B) and one capacitor (C). The capacitor charges and discharges between 1/3 V_{cc} and 2/3 V_{cc} (with V_{cc}=12V). Charge (*output high*) and discharge times (*output low*) are respectively given by:

$$t_1 = 0.693\ (R_A + R_B)\ C$$

$$t_2 = 0.693\ (R_B)\ C$$

Thus, the total period of the control is given by:

$T = t_1 + t_2$

A non-stop two-hour test was carried out. Signal *rms* was computed each 6-sec time interval (Figure 13, red line). Results showed a quite good steady system performance.

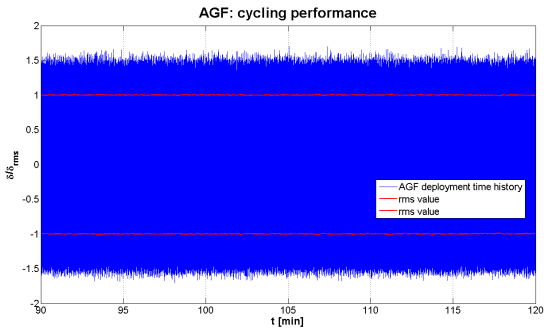

Figure 13: AGF cycling test

One-second time records, Figure 14, show the presence of high frequency components, over the main carrier signal. The difference between upper and lower lobes seems to indicate some slight non-linearity in the assembled set-up. In particular, the upper stroke end of the beam seemed to be not rigid enough.

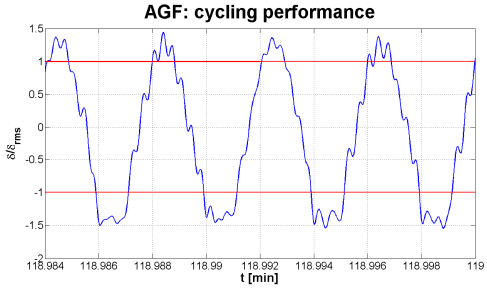

Figure 14: AGF cycling tests (zoom)

The signal FFT, Figure 15, indicates a clear peak at about 4Hz, the excitation frequency. Other minor peaks do appear at the first beam bending mode (about 6Hz), at the excitation frequency harmonics and other frequencies, resulting from the non-linear features of the investigated system.

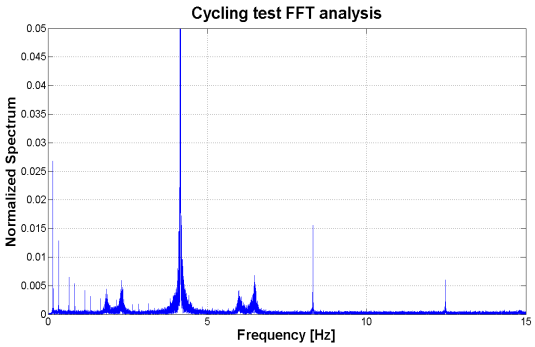

Figure 15: AGF deployment FFT

CONCLUSIONS

An original and innovative AGF concept was proposed and developed from the Smart Structures Lab of the Italian Aerospace Research Centre (CIRA).

The actuation system is based on the use of a cantilever flapped beam, forced by electromagnet devices. Herein, the authors demonstrated the possibility to produce the desired structural dynamic response with a limited electrical power consumption (about 5W) and a low weight penalty (about 50 gr).

The originality and advantages of the proposed concept relies in the possibility of attaining the targeted performance with a very simple structure. Taking advantage of the beam elasticity, required dynamics can be obtained without any kind of amplification and kinematic systems. This is a formidable advantage when considering the effects of the centrifugal field, typical of an operative helicopter rotor blade environment. Presented analysis was focused on the proposed device protrusion time.

In the experiments, a certain discrepancy was shown both in terms of numerical and experimental correlation. This was due to the difficulty of reaching the ideal condition in terms of mechanical and electrical losses. Nevertheless, the attained performance was always close to fixed requirements. Specific set-up refinements are expected to improve the quality of dynamic response

In future activities, an optimization numerical process will be carried out to fix magneto-mechanical and geometrical characteristics and a DSP-based closed loop control system will be implemented. A specific test rig will also be assembled to test system behaviour under a simulated centrifugal effect.

AKNOWLEDGMENTS

This research activity is funded by the Clean Sky Joint Undertaking under projects GAM-GRC, related to activities performed within the ITD Green Rotorcraft.

The authors would also like to thank Dr. Salvatore Ameduri for his guide in the very first approach to FEMM4.2 software and Mr. Antonio Calabrò for his support in the experimental setup realisation.

REFERENCES

[1] Liebeck, R. H., “Design of Subsonic Airfoils for High Lift,” Journal of Aircraft , Vol. 15, No. 9, September 1978, pp. 547–561.

[2] Yee, K., Joo, W., Lee, D.-H., Aerodynamic performance analysis of a Gurney flap for rotorcraft application, (2007) Journal of Aircraft, 44 (3), pp. 1003-1014.

[3] Claude G. Matalanis and John K. Eaton, “Wake Vortex Alleviation Using Rapidly

Actuated Segmented Gurney Flaps", Report No. 102 Flow Physics and Computation Division Department of Mechanical Engineering Stanford University Stanford, CA 94305-3030 January 2007.

[4] E.A. Mayda, C.P. van Dam, D. Yen Nakafuji, "Computational Investigation of Finite Width Microtabs for Aerodynamic Load Control", AIAA-2005-1185.

[5] Tianshu Liu and J. Montefort, "Thin-Airfoil Theoretical Interpretation for Gurney Flap Lift Enhancement", Journal of Aircraft, Vol. 44, No. 2, March–April 2007.

[6] J.J. Wang, Y.C. Li, K.-S. Choi, "Gurney flap-Lift enhancement, mechanisms & applications", Progress in Aerospace Sciences, Volume 44, Issue 1, January 2008, Pages 22-47.

[7] M. S. Chandrasekhara, "Lost-Lift Recovery in Compressible Dynamic Stall Control Using a Gurney Flap", Proc. of the International Conference on Aerospace Science and Technology 26-28 June 2008, Bangalore, India.

[8] A. Paternoster , P. de Jong, R. Loedersloot, A. de Boer, R. Akkerman, Initial Technology Review, IGOR - Actuator and Control System for Green Rotorcraft I.T.D., University of Twente, Engineering Technology, 2009. [http://doc.utwente.nl/69643/1/Piezo_actuators_Gurney_flaps_2-2.pdf].

[9] G. Diodati, M. Ciminello, A. Concilio, "Technological Solutions for Realising an Active Gurney Flap for Green Rotorcraft Applications, Based on Piezoelectrics and Electromagnets", Proceedings of the ASME 2011 Conference on Smart Materials, Adaptive Structures and Intelligent Systems SMASIS2011 September 18-21, 2011, Scottsdale, Arizona, USA.

[10] Van Dam et al., "Microfabricated Translational Stages for Control of Aerodynamic Loading", US Patent N. 7,028,954 B2, Apr. 18, 2006.

[11] Kentfield, J. A. C., "The Potential of Gurney Flaps for improving the Aerodynamic Performance of Helicopter Rotors," Paper AIAA 1993-4883, AIAA International Powered Lift Conference Proceedings, Santa Clara, CA, December 1–3, 1993.

[12] Maughmer, M., Lesieutre, G., and Kinzel, M., "Miniature Trailing-Edge Effectors for Rotorcraft Performance Enhancement," American Helicopter Society 61st Annual Forum Proceedings, Grapevine, TX, June 1–3, 2005.

[13] Myose, R., Papadakis, M., and Heron, I., "Gurney Flap Experiments on Airfoils, Wings, and Reflection Plane Model," Journal of Aircraft, Vol. 35, (2), March–April 1998, pp. 206–211.

[14] www.femm.info.

[15] www.cei-italy.it.